Available online at www.sciencedirect.com
ScienceDirect
Journal of Power Sources 178 (2008) 373–378
JOURNAL OF POWER SOURCES
www.elsevier.com/locate/jpowsour

Short communication

Microstructural evolution of NbF_5-doped MgH_2 exhibiting fast hydrogen sorption kinetics

Ji Woo Kim [a,b], Jae-Pyoung Ahn [c,*], Seon-Ah Jin [b], Sang Hoon Lee [a], Hee-Suk Chung [a], Jae-Hyeok Shim [b], Young Whan Cho [b], Kyu Hwan Oh [a]

[a] *Department of Materials Science and Engineering, Seoul National University, Seoul 151-742, Republic of Korea*
[b] *Materials Science and Technology Research Division, Korea Institute of Science and Technology, Seoul 136-791, Republic of Korea*
[c] *Advanced Analysis Center, Korea Institute of Science and Technology, Seoul 136-791, Republic of Korea*

Received 12 November 2007; received in revised form 1 December 2007; accepted 3 December 2007
Available online 14 December 2007

Abstract

The microstructure of MgH_2 with 1 mol% NbF_5, prepared by high-energy ball milling (HEBM), was studied using high resolution transmission electron microscopy (HR-TEM) with an X-ray energy dispersive spectrometer (EDS) before and after hydrogen sorption cycles. The TEM samples were prepared without any air exposure by a novel, focused ion beam (FIB) system specially designed for highly air sensitive materials. During HEBM, the doping agent, NbF_5, was distributed as an extremely thin, film-like, amorphous phase along the grain boundaries of the nanocrystalline MgH_2. After 10 sorption cycles, amorphous Nb-F phase was transformed into crystalline Nb hydrides. It is believed that the Nb hydride played a decisive role in improving the sorption kinetics of MgH_2.

Keywords: Hydrogen storage; Hydrides; Transmission electron microscopy; Focused ion beam; Catalysts

1. Introduction

Efficient and safe hydrogen storage is one of the key components of a practical hydrogen economy [1]. Due to its light weight, low cost and excellent gravimetric and volumetric storage capacity, metal hydride is a promising alternative to the physical methods such as compression or liquefaction of hydrogen. Among the various light metal hydrides, MgH_2 is one of the most promising for on-board applications because of its very high hydrogen capacity up to a theoretically limit of 7.6 wt%. However, the equilibrium dehydrogenation temperature is high, at 290 °C under 1 bar of hydrogen, and the sorption kinetics are unacceptably slow. These are the main obstacles to overcome before MgH_2 can be seriously considered as one of the practical materials for high capacity, solid-state hydrogen storage systems.

Previous studies have shown that the hydrogen sorption properties of nanocrystalline MgH_2 fabricated by high-energy ball milling (HEBM) are significantly improved [2,3]. Recently, it has been reported that MgH_2-5 at.%Nb nanocomposites have very fast hydrogen sorption kinetics [4–6] and that MgH_2-5 at.%NbH nanocomposites exhibit enhanced hydrogen desorption kinetics [7]. Checchetto et al. [8] suggested that the catalytic action of Nb in the hydrogen sorption kinetics is connected with the formation of nano-sized Nb clusters dispersed in the MgH_2 matrix. More recently, it has been shown that the addition of transition metal fluorides, such as FeF_3 and NiF_2, improves the hydrogen sorption kinetics of MgH_2 [9–11]. We have recently found that the addition of a small amount of NbF_5 significantly improves the sorption kinetics of MgH_2 and have suggested that the extremely fine and surface oxide-free Nb hydrides that are formed in situ during ball milling and/or hydrogenation processes will act as an effective catalyst [12].

A number of transmission electron microscopy (TEM) studies have investigated the structure of catalysts in MgH_2 [6,8,13,14] and complex metal hydrides such as $NaAlH_4$ [15–17] and $LiAlH_4$ [18], which are further promising candidates for hydrogen storage materials. However, it is extremely difficult to prepare TEM samples due to the high air sensitivity of these materials. Moreover, the observation areas are

* Corresponding author. Tel.: +82 2 958 5536; fax: +82 2 958 5529.
E-mail address: jpahn@kist.re.kr (J.-P. Ahn).

0378-7753/$ – see front matter © 2007 Elsevier B.V. All rights reserved.
doi:10.1016/j.jpowsour.2007.12.005

limited to the particle edges, because powder samples have three-dimensional particle shapes. Focused ion beam (FIB) makes it possible to prepare uniformly thin TEM samples which have a wide observable area. By applying this method, we have improved the FIB system with an air-lock loading chamber to prepare TEM samples without any air exposure. Using analytical TEM, we closely investigated the nature of NbF_5 in MgH_2, which may help in realizing the potential of MgH_2 for practical use in on-board hydrogen storage applications.

2. Experimental

98% NbF_5 and 98% MgH_2 were purchased from Aldrich and Alfa Asear, respectively. One gram of MgH_2 containing 1 mol% of NbF_5 was charged with ten 7.9 mm diameter Cr-steel balls into a 70 ml hardened steel vial and milled for 15 min by a SPEX-8000 vibratory mill. All the sample handlings were done in a glove box under argon atmosphere. Both the oxygen and water vapor levels inside the glove box were kept below 1 ppm. The phase composition of the as-milled sample was measured by an X-ray diffractometer (XRD, Bruker, D8 Advance) with Cu Kα radiation. A special air tight sample holder was used to prevent any possible reactions between the sample and air during XRD measurement.

For the electron microscopy analysis, powder samples in a glove box were transferred into FIB using an attachable, air-lock loading chamber. As can be seen in Fig. 1, the cross-sectional TEM samples were obtained from the specific interest region of both powders as-milled and after 10 sorption cycles by dual-beam FIB (FEI, Nova 200). The Pt protective layer was deposited on an NbF_5-doped MgH_2 particle with 2 μm thickness using 0.1–0.3 nA ion beam currents (Fig. 1(a)) and the particle was sectioned both front and back side by 30 keV Ga^+ ions beam (Fig. 1(b)). A cross-sectional sample of 10 μm × 5 μm × 0.1 μm was produced by the lift-out technique [19] and was attached to a TEM Cu grid using a manipulating probe (100.7^{TM}, Omniprobe) as can be seen in Fig. 1(c and d). Further thinning of the lifted-out sample to electron transparency was performed by milling parallel to the cross-sectional plane with low ion beam currents (30–50 pA) down to a final sample thickness of 50–90 nm. After final ion milling, the TEM sample was transferred back to the glove box, using the attachable air-lock loading chamber, and placed in anhydrous toluene, with a relative evaporation rate of 6.1 (where ether = 1), as an air protective layer. The soaked TEM sample was loaded into a 200 keV transmission electron microscope (FEI, Tecnai F20) equipped with an X-ray energy dispersive spectrometer (EDS) without air exposure. Scanning transmission electron microscope (STEM) bright field images were collected using a high-angle annular dark-field (HAADF) detector. Crystallographic information was obtained by high resolution TEM (HR-TEM) micrographs and selected area electron diffraction (SAED) pattern, followed

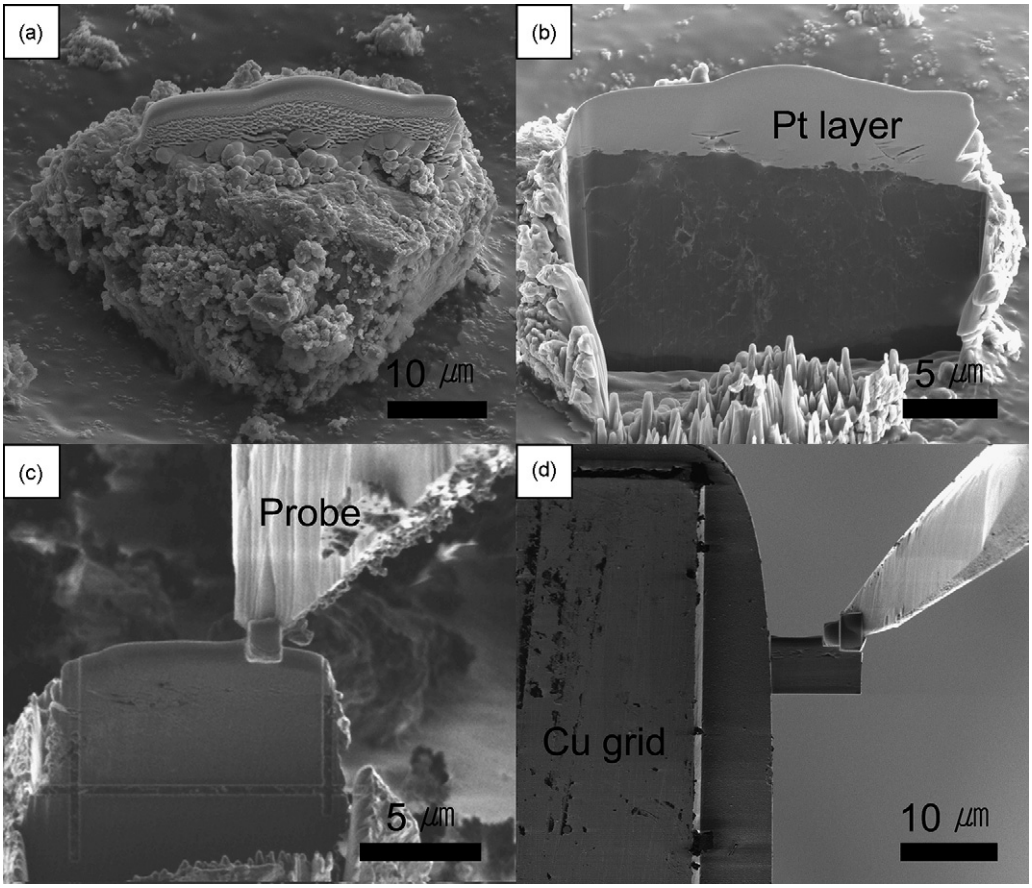

Fig. 1. Sequence of cross-sectional TEM sample peparation by FIB: (a) deposition of Pt protective layer, (b) one side view of a thin membrane trenched by Ga^+ ion irradiation, (c) U-cut and lift-out of the membrane using a manipulating probe, and (d) attachment to a Cu grid for TEM observation.

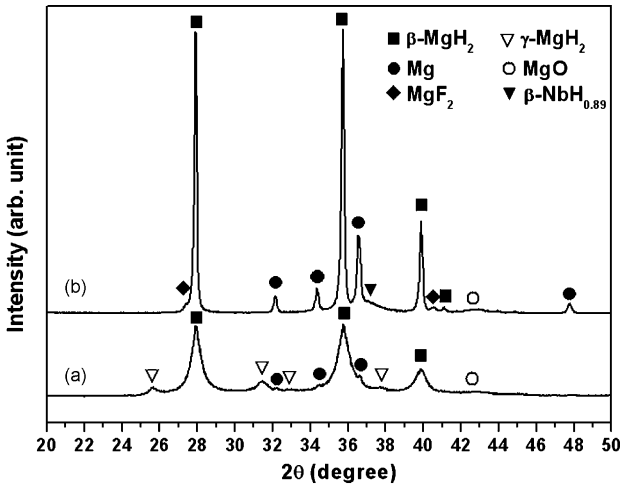

Fig. 2. XRD patterns of MgH_2 with 1 mol% NbF_5: (a) as milled for 15 min and (b) after 10 hydrogen sorption cycles.

by analysis with the software package (Gatan, Digital Micrograph).

3. Results and discussion

Fig. 2(a) shows the XRD pattern of MgH_2 powder ball milled for 15 min with 1 mol% NbF_5. Both tetragonal β-MgH_2 (PDF No. 74-0934) and orthorhombic γ-MgH_2 (PDF No. 35-1184) were observed, together with small amounts of Mg and MgO, which were also detected in the as-received MgH_2 (β-MgH_2 tetragonal structure). The estimated crystallite size of tetragonal β-MgH_2 derived by the Scherrer's formula [20] taking into account the instrumental broadening was about 20 nm. The formation of a highly reactive and protective MgF_2 surface layer by F-treatment has been proposed for Mg-based alloys [21]. Also, it has been recently suggested that a MgF_2 surface layer, which has a high affinity to hydrogen, and transition metal nanoparticles are produced by a displacement reaction between MgH_2 and transition metal fluoride catalyst during ball mill, and that these products activate the hydrogen desorption of MgH_2 [9–11]. However, the diffraction peaks of MgF_2 and Nb phases were not clearly detected in this XRD pattern due to their small volume fraction.

After 10 sorption cycles, we found tetragonal MgF_2 (PDF No. 72-2231) and broad β-$NbH_{0.89}$ (PDF No. 07-0263) peaks in the XRD pattern (Fig. 2(b)). It can be inferred that during sorption cycles a displacement reaction between MgH_2 and Nb-F takes place producing MgF_2 and a very fine Nb phase, and that through the hydrogen absorption process Nb is transformed into metastable β-$NbH_{0.89}$ phase [22,23]. After 10 sorption cycles, metastable γ-MgH_2 is transformed into stable tetragonal β-MgH_2 and the crystallite size of β-MgH_2 increases to ~100 nm.

SEM micrographs of both specimens, as-milled and after 10 sorption cycles, are presented. As can be seen in Fig. 3(a), an enlargement image of the as-milled MgH_2 powders with 1 mol% NbF_5 indicates that particles consist of smooth shapes and dense surface with a broad particle size ranging from 15 to 50 μm. As shown in Fig. 3(b), after 10 sorption cycles primary particles with 0.5–3 μm were observed and small pores were also generated between the aggregates of the primary particles. During hydrogen desorption, MgH_2 transforms into Mg and the unit cell volume of MgH_2 is reduced by 25% (unit cell volume of MgH_2: 61.62 $Å^3$ and Mg: 46.48 $Å^3$). Therefore, the pore generation and small particles are attributed to the repeated volume shrinkage and expansion during sorption cycles.

Here, the microstructural and compositional characterization of Nb fluoride can not be revealed because a large interaction volume between electrons and samples in SEM. Therefore, the overall chemical composition and the distribution of catalyst which is known as a key factor for the enhanced kinetics will be given clearly at Fig. 4 with a cross-sectional view by TEM.

Fig. 4(a) is a cross-sectional HAADF image of the as-milled MgH_2 with 1 mol% NbF_5 sample where a relatively heavy weighted phase appears with bright contrast. Indexing of the SAED pattern (Fig. 4(b)) obtained from point 2 shows that β-MgH_2 is the main crystalline phase and in particular, γ-MgH_2 phase is formed during HEBM. In the HR-TEM image (Fig. 4(c)), the measured crystallite size of the tetragonal β-MgH_2 phase varies between 20 and 40 nm, which agrees with the XRD analysis result (~20 nm). The HR-TEM image also

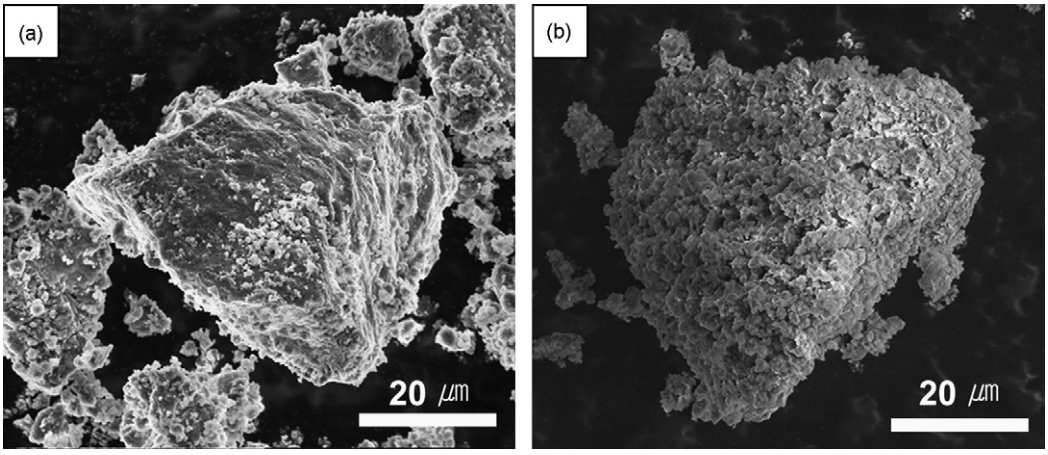

Fig. 3. SEM images of MgH_2 with 1 mol% NbF_5 catalyst: (a) as-milled for 15 min and (b) after 10 hydrogen sorption cycles.

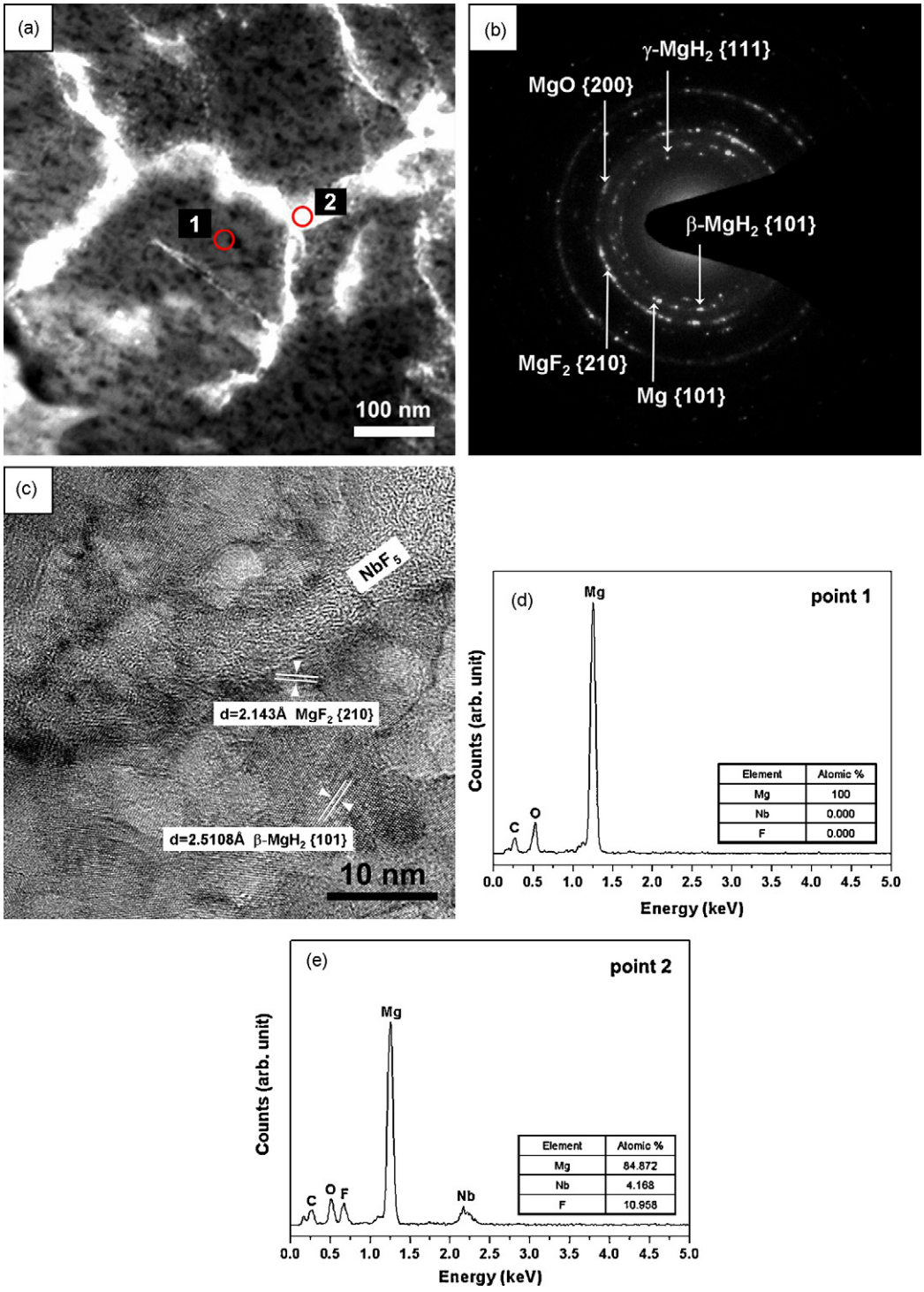

Fig. 4. (a) Cross-sectional HAADF-STEM image of as-milled MgH_2 (gray color) with 1 mol% NbF_5 (white color) after ball milling time of 15 min, (b) SAED pattern from point 2, (c) cross-sectional HR-TEM image of point 2 (NbF_5 rich region) indicating a NbF_5 amorphous layer, MgF_2 cubic phase at the MgH_2/NbF_5 interface and nanocrystalline β-MgH_2; and EDS spectra from (d) point 1, and (e) point 2.

demonstrates that the added catalyst NbF_5 exists as amorphous structure. There was no evidence in the XRD pattern to support the reaction between MgH_2 and NbF_5 for the production of MgF_2 (Fig. 2(a)). However, the SAED pattern (Fig. 4(b)) and the HR-TEM image (Fig. 4(c)) reveal that the MgF_2 phase with a cubic structure (PDF No. 38-0882) [24] was formed as a result of the local reaction at the MgH_2/NbF_5 interface during HEBM. This cubic MgF_2 phase is known to be stable under the high pressure and temperature condition which can be locally developed during HEBM. As previously reported [21], MgF_2 is believed to improve the initial activation of NbF_5-doped MgH_2 in the hydrogen desorption process. Fig. 4(d and e) show EDS spectra

from points 1 and 2, and their quantitative chemical composition in the inset tables. It can be inferred that MgH_2 particles (point 1) with size range about 200–500 nm are surrounded by the Nb-F layer of 10–30 nm thickness (point 2). It means that the Nb-F catalyst with a network structure made lots of interface between fine MgH_2 matrix and thin film-like Nb-F catalyst achieved by HEBM. It is suggested that these morphologies lead to the significant improvement in the hydrogen sorption kinetics of the NbF_5-doped MgH_2.

The microstructure and chemical composition of the specimen after 10 sorption cycles are analyzed in Fig. 5. As presented in Fig. 5(a), the bright contrast phase, which is indicated by point 2, was well distributed as thin layers along grain boundaries with a thickness of 10–30 nm. From the SAED pattern

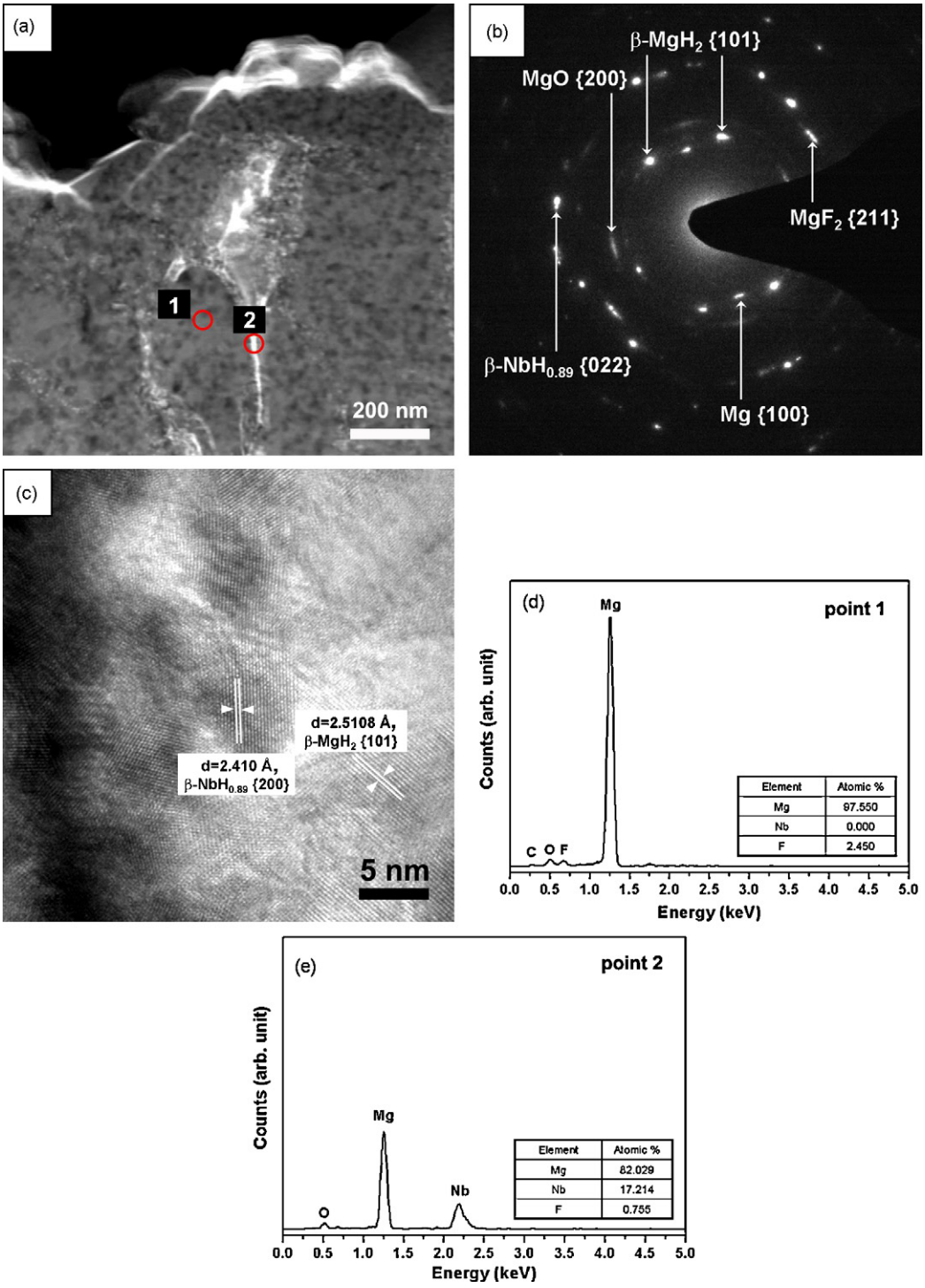

Fig. 5. (a) Cross-sectional HAADF-STEM image of MgH_2 with 1 mol% NbF_5 after 10 hydrogen sorption cycles showing MgH_2 particles (gray color) and Nb hydride layer (white color), (b) SAED pattern from point 2, (c) cross-sectional HR-TEM image of point 2 (Nb hydride rich region) indicating a Nb hydride (β-$NbH_{0.89}$) layer and crystalline β-MgH_2; and EDS spectra from (d) point 1, and (e) point 2.

(Fig. 5(b)) and the HR-TEM image (Fig. 5(c)) at point 2, the bright thin layer along the grain boundaries was identified as a β-$NbH_{0.89}$ crystalline phase. It is well known that Nb can dissolve a considerable amount of hydrogen (up to [H]/[Nb] = 2) and that a large variety of different phases can form [25]. Moreover, hydrogen diffuses rapidly in Nb metal [26]. Therefore, it is believed that the Nb crystalline layer on the surface of the MgH_2 particles effectively releases and uptakes hydrogen gas during the hydrogen sorption process and ultimately improves the hydrogen sorption kinetics of MgH_2. In addition, the layer seems to act as an impediment to the MgH_2 particle growth. From the EDS spectra of point 1 and 2 (Fig. 5(d and e)), it can be inferred that some of the F element originating from Nb-F is dissolved into the MgH_2 structure during the sorption cycles. Recent studies have shown that F ion is soluble in some alkali metal hydrides [27,28]. Over saturated F is likely to form the MgF_2 tetragonal phase in the MgH_2 matrix (as can be seen in Fig. 2(b)). Before and after hydrogen sorption cycles, the local atomic ratio of Mg/F and Nb/F at the each region (see the inset tables in Fig. 4(d and e) and Figs. 5(d and e)) also proves the migration of F to the MgH_2 matrix and the SAED pattern (Fig. 5(b)) supports the formation of tetragonal MgF_2. This unique microstructure, consisting of an in situ formed Nb layer (Nb hydrides at the absorption state) and MgF_2 phases (cubic and tetragonal) during ball milling and/or hydrogenation processes, might play a crucial role in improving the sorption kinetics of MgH_2.

4. Conclusion

In summary, the TEM analyses of the composite MgH_2-1 mol% NbF_5 prepared by ball milling indicated the presence of a Nb hydride film layer on the surface of the MgH_2 particles and of a MgF_2 phase in the MgH_2 matrix. The Nb hydride layer would be responsible of the improvement of the H sorption kinetics of MgH_2. This hydride coating was also believed to suppress the grain growth of nanocrystalline MgH_2 quite effectively and thus maintain its initial catalytic activity throughout repeated hydrogen sorption cycles. The MgF_2 byproduct formed by fluorine transfer reaction during ball milling and hydrogen sorption cycles was decisive for initial activation of the hydrogen desorption of MgH_2.

Acknowledgement

This work has been supported by the Hydrogen Energy R&D Center, one of the 21st Century Frontier R&D Programs, funded by the Ministry of Science and Technology of Korea.

References

[1] L. Schlapbach, A. Zuttel, Nature 414 (2001) 353.
[2] L. Zaluski, A. Zaluska, J.O. Ström-Olsen, J. Alloys Compd. 253 (1997) 70.
[3] J. Huot, G. Liang, S. Boily, A. Van Neste, R. Schulz, J. Alloys Compd. 293 (1999) 495.
[4] J.F. Pelletier, J. Huot, M. Sutton, R. Schulz, A.R. Sandy, L.B. Lurio, S.G.J. Mochrie, Phys. Rev. B 63 (2001) 052103.
[5] J. Huot, J.F. Pelletier, L.B. Lurio, M. Sutton, R. Schulz, J. Alloys Compd. 348 (2003) 319.
[6] J.F.R. de Castro, S.F. Santos, A.L.M. Costa, A.R. Yavari, W.J.F. Botta, T.T. Ishikawa, J. Alloys Compd. 376 (2004) 251.
[7] A.R. Yavari, J.F.R. de Castro, G. Vaughan, G. Heunen, J. Alloys Compd. 353 (2003) 246.
[8] R. Checchetto, N. Bazzanella, A. Miotello, C. Maurizio, F. D'Acapito, P. Mengucci, G. Barucca, G. Majni, Appl. Phys. Lett. 87 (2005) 061904.
[9] S. Deledda, A. Borissova, C. Poinsignon, W.J. Botta, M. Dornheim, T. Klassen, J. Alloys Compd. 404 (2005) 409.
[10] J.F.R. de Castro, A.R. Yavari, A. LeMoulec, T.T. Ishikawa, W.J.F. Botta, J. Alloys Compd. 389 (2005) 270.
[11] A.R. Yavari, A. LeMoulec, F.R. de Castro, S. Deledda, O. Friedrichs, W.J. Botta, G. Vaughan, T. Klassen, A. Fernandez, Åř. Kvick, Scripta Mater. 52 (2005) 719.
[12] S.-A. Jin, J.-H. Shim, J.-P. Ahn, Y.W. Cho, K.-W. Yi, Acta Mater. 55 (2007) 5073.
[13] O. Friedrichs, J.C. Sanchez-Lopez, C. Lopez-Cartes, T. Klassen, R. Bormann, A. Fernandez, J. Phys. Chem. B 110 (2006) 7845.
[14] N. Hanada, E. Hirotoshi, T. Ichikawa, E. Akiba, H. Fujii, J. Alloys Compd., in press.
[15] M. Felderhoff, K. Klementiev, W. Grunert, B. Spliethoff, B. Tesche, J.M. von Colbe, B. Bogdanovic, M. Hartel, A. Pommerin, F. Schuth, C. Weidenthaler, Phys. Chem. Chem. Phys. 6 (2004) 4369.
[16] C.M. Andrei, J.C. Walmsley, H.W. Brinks, R. Holmestad, S.S. Srinivasan, C.M. Jensen, B.C. Hauback, Appl. Phys. A 80 (2005) 709.
[17] A. Leon, O. Kircher, H. Rosner, B. Decamps, E. Leroy, M. Fichtner, A. Percheron-Guegan, J. Alloys Compd. 414 (2006) 190.
[18] C.M. Andrei, J. Walmsley, D. Blanchard, H.W. Brinks, R. Holmestad, B.C. Hauback, J. Alloys. Compd. 395 (2001) 307.
[19] L.A. Giannuzzi, J.L. Drown, S.R. Brown, R.B. Irwin, F.A. Stevie, Microsc. Res. Tech. 41 (1998) 285.
[20] B.D. Cullity, S.R. Stock, Elements of X-ray Diffraction, third ed., Prentice Hall, London, 2001, p. 167.
[21] F.-J. Liu, S. Suda, J. Alloys. Compd. 231 (1995) 742.
[22] J. Huot, J.F. Pelletier, G. Liang, M. Sutton, R. Schulz, J. Alloys Compd. 330–332 (2002) 727.
[23] T. Schober, Vanadium-, niobium- and tantalum-hydrogen, in: F.A. Lewis, A. Aladjem (Eds.), Hydrogen Metal Systems I Solid State Phenomena, Scitec, Zurich, 1996, p. 357.
[24] L. Ming, M.H. Manghnana, Geophys. Res. Lett. 6 (1979) 13.
[25] T. Schober, H. Wenzel, in: G. Alefeld, J. Völkl (Eds.), In Hydrogen in Metals II, Topics in Applied Physics Vol. 29, Springer-Verlag, Berlin, Heidelberg, New York, 1978, p. 11.
[26] R. Hempelmann, J. Less Common Met. 101 (1984) 64.
[27] E.H. Majzoub, J.L. Herberg, R. Stumpf, S. Spangler, R.S. Maxwell, J. Alloys. Compd. 394 (2005) 265.
[28] L.-C. Yin, P. Wang, X.-D. Kang, C.-H. Sun, H.-M. Cheng, Phys. Chem. Chem. Phys. 9 (2007) 1499.